Journal of Pathology
J Pathol November 2024; **264:** 318–331
Published online 27 September 2024 in Wiley Online Library
(wileyonlinelibrary.com) DOI: 10.1002/path.6351

ORIGINAL ARTICLE

TERT upregulation promotes cell proliferation via degradation of p21 and increases carcinogenic potential

Masako Mishima[1], Atsushi Takai[1]*, Haruhiko Takeda[1], Eriko Iguchi[1], Shigeharu Nakano[1], Yosuke Fujii[1], Masayuki Ueno[1], Takahiko Ito[1], Mari Teramura[1], Yuji Eso[1], Takahiro Shimizu[1], Takahisa Maruno[1], Shizu Hidema[2], Katsuhiko Nishimori[2], Hiroyuki Marusawa[3], Etsuro Hatano[4] and Hiroshi Seno[1]

[1] *Department of Gastroenterology and Hepatology, Graduate School of Medicine, Kyoto University, Kyoto, Japan*
[2] *Department of Bioregulation and Pharmacological Medicine, Fukushima Medical University, Fukushima, Japan*
[3] *Department of Gastroenterology and Hepatology, Osaka Red Cross Hospital, Osaka, Japan*
[4] *Department of Surgery, Graduate School of Medicine, Kyoto University, Kyoto, Japan*

**Correspondence to: A Takai, Department of Gastroenterology and Hepatology, Graduate School of Medicine, Kyoto University, 54 Kawahara-cho, Shogoin, Sakyo-ku, Kyoto 606-8507, Japan. E-mail: atsushit@kuhp.kyoto-u.ac.jp*

Abstract

Telomerase reverse transcriptase (*TERT*) gene aberration is detectable in >80% of cases with hepatocellular carcinoma (HCC). TERT reactivation is essential for cellular immortalization because it stabilizes telomere length, although the role of TERT in hepatocarcinogenesis remains unelucidated. To elucidate the significance of aberrant TERT expression in hepatocytes in inflammation-associated hepatocarcinogenesis, we generated *Alb-Cre;Tert*Tg mice, which overexpress TERT in the liver and examined their phenotype during chronic inflammation. Based on transcriptome data from the liver tissue of *Alb-Cre;Tert*Tg mice, we examined the role of TERT in hepatocarcinogenesis *in vitro*. We also evaluated the relationship between TERT and cell-cycle-related molecules, including p21, in HCC samples. The liver tumor development rate was increased by TERT overexpression during chronic inflammation, especially in the absence of p53 function. Gene set enrichment analysis of liver tissues revealed that gene sets related to TNF-NFκB signaling, cell cycle, and apoptosis were upregulated in *Alb-Cre;Tert*Tg liver. A luciferase reporter assay and immunoprecipitation revealed that TERT interacted with NFκB p65 and enhanced NFκB promoter activity. On the other hand, TERT formed protein complexes with p21, cyclin A2, and cyclin E and promoted ubiquitin-mediated degradation of p21, specifically in the G1 phase. In the clinical HCC samples, TERT was highly expressed but p21 was conversely downregulated, and TERT expression was associated with the upregulation of molecules related to the cell cycle. Taken together, the aberrant upregulation of TERT increased NFκB promoter activity and promoted cell cycle progression via p21 ubiquitination, leading to hepatocarcinogenesis.

Keywords: hepatocellular carcinoma; cell cycle; liver cancer; carcinogenesis; hepatocyte; tert; mouse models

Received 16 December 2023; Revised 13 June 2024; Accepted 16 August 2024

No conflicts of interest were declared.

Introduction

Liver cancer is the second most lethal tumor in terms of 5-year survival [1] and will affect an estimated one million people each year by 2025 [2]. Hepatocellular carcinoma (HCC) accounts for >90% of all liver cancers and often occurs in the context of accumulated genetic mutations caused by chronic hepatitis or cirrhosis [3]. Although the comprehensive analysis of genetic alterations in HCC has been extensively performed using high-throughput next-generation sequencing technologies [1,4], the functional significance of gene aberrations previously reported in hepatocarcinogenesis remains unclear.

The most frequently altered gene in HCC is telomerase reverse transcriptase (*TERT*) encoding a component of telomerase [5,6], a ribo-nucleo protein composed of multiple components that protects telomeres from shortening by repairing their ends after every round of cell division [7–10]. *TERT* aberrations, including promoter mutations, hepatitis B virus (HBV) integrations, chromosomal translocations, and promoter methylation [11–13], have been reportedly found in >80% of cases of HCC [4,14]. Most of these alterations lead to the re-expression of the *TERT* gene, which is transcriptionally silenced in normal differentiated somatic cells [7]. *TERT* gene aberration has already been found in 19% of cases at the stage of precancerous dysplastic nodule, and the frequency of the mutations increases up to 61% in early-stage, well-differentiated HCC [15]. We previously reported that regenerative nodules harbored no *TERT* promoter mutations and showed levels of TERT

expression comparable to those of normal liver tissues. However, HCC tissues with *TERT* aberrations showed unexceptionally high levels of gene expression, for example, eight- to 100-fold for promoter mutation and several hundred- to several thousand-fold for structural variation in gene loci [11,16]. In addition, we recently detected types of *TERT* gene aberrations as trunk mutations during multistep hepatocarcinogenesis through the whole-genome sequencing analysis of HCC samples collected by a multiregional sampling method [11]. These results suggest that *TERT* gene aberration is the initial step in hepatocarcinogenesis.

Although *TERT* gene aberrations are a major feature of hepatocarcinogenesis as described earlier, its biological significance has not been sufficiently examined. Aberrant reactivation of telomerase has been considered to induce cell immortalization by protecting the ends of telomeres from critical shortening [7]. However, it is not clear whether the re-expression of TERT fuels the early stages of hepatocarcinogenesis before telomeres are shortened to a critical degree. Notably, several studies have indicated that telomerase affects not only telomere repair but also other molecular functions, such as the activation of oncogenic pathways and changes in mitochondria metabolism [17–19].

In the current study, we generated a mouse model of liver specific *Tert* overexpression and examined the phenotype under chronic inflammation recapitulating the clinical course of human hepatocarcinogenesis. We identified a novel role of TERT in driving cell cycle progression via p21 ubiquitination, independent of telomere maintenance, which could explain why TERT gene aberrations, leading to its upregulation, frequently occur in the very early phase of hepatocarcinogenesis.

Materials and methods

Mice

All mice used in this study were housed in a specific pathogen-free, temperature-controlled facility with 12-h light/dark cycles at the Kyoto University Faculty of Medicine. Male and female TERT conditional transgenic mice (*Tert*cTg) with a C57/BL6 background were self-crossed to obtain transgenic mice [20]. The *Alb-Cre* mice were provided by the Center for iPS Cell Research and Application (Kyoto University, Kyoto, Japan) [21]. The *Trp53*-floxed mice were purchased from the Jackson Laboratory (JAX strain 008462; Farmington, CT, USA). The primers used for PCR genotyping are listed in supplementary material, Table S1.

Animal experiments

Thioacetamide (TAA) (Sigma-Aldrich, St. Louis, MO, USA) was dissolved in drinking water at a concentration of 0.02%, starting at the age of 8–10 weeks. Before tissue collection, animals were anesthetized by injecting at a concentration of 30 μg/mg chloral hydrate (NACALAI TESQUE, Kyoto, Japan) peritoneally. All animal experiments were approved by the Ethics Committee for Animal Experiments and performed (Approval No. 23167) according to the Guidelines for Animal Experiments of Kyoto University.

Human samples

Human HCC samples surgically resected from 2 cases at the Kyoto University Hospital were used for immunohistochemistry. Written informed consent or an opt-out consent was obtained from all participants. This study conformed to the provisions of the Declaration of Helsinki, and the study protocol was approved by the Ethics Committee of Kyoto University (G1317).

Histology and immunohistochemistry

Details are presented in Supplementary materials and methods. The antibodies used in this study are listed in supplementary material, Table S2.

Reverse transcription-quantitative polymerase chain reaction (RT-qPCR)

Quantitative real-time PCR was performed on a LightCycler 96 System (Roche, Basel, Switzerland) using the primers listed in supplementary material, Table S3.

RNA sequencing

After passing a strict quality check, each library was constructed using TruSeq RNA Sample Prep Kit v2 (Illumina, San Diego, CA, USA) according to the manufacturer's instructions. RNA sequencing (RNA-seq) was performed using the NovaSeq 6000 (Illumina) platform. RNA-seq generated 100-bp paired-end sequences that were aligned to the reference genome sequence (GRCh37 or GRCm38). Sequence data analyses, including alignment and raw read counts, were performed using the Genomon2 pipeline (version 2.6) [22,23]. The expression level of each gene was normalized using the TMM algorithm, and differentially expressed genes (DEGs) were extracted using edgeR [24].

Gene set enrichment analysis and pathway analysis

Gene set enrichment analysis (GSEA) and pathway analysis were performed on GSEA 3.0 software (Broad Institute, Cambridge, MA, USA) with 1,000 gene-set permutations [25] using the gene-ranking metric *t*-test with mouse-ortholog hallmark and Kyoto Encyclopedia of Genes and Genomes (KEGG) collection and the Database for Annotation, Visualization and Integrated Discovery (DAVID 6.8) using the public software obtained from the Broad Institute [26].

DNA extraction and measurement of telomere length of liver cells

The telomere length of the liver cells was measured using Absolute Telomere Length Quantification qPCR

Assay Kit (ScienCell Research Laboratories, Carlsbad, CA, USA) following the manufacturer's protocol.

Western blotting and co-immunoprecipitation

The details are presented in Supplementary materials and methods. The antibodies used in this study are listed in supplementary material, Table S2.

Cell culture and transfection

Human hepatoma-derived cell lines, HepG2 and Huh7.5 cells, were obtained from the Institute for Virus Research, Kyoto University (Kyoto, Japan), and Huh7 was obtained from RIKEN (Yokohama, Japan). All these cell lines were authenticated by short-tandem repeat analysis at the JCRB Cell Bank, National Institute of Biomedical Innovation (Osaka, Japan). Details are presented in Supplementary materials and methods.

Cell proliferation assay and cell cycle analysis

Cell cycle analyses were performed using a BrdU kit (BioLegend, San Diego, CA, USA) following the manufacturer's instructions. Details are presented in Supplementary materials and methods.

Isolation and culture of murine primary hepatocyte

Primary hepatocytes were cultured as described previously [27].

Luciferase assay

The reporter plasmid assay was performed as reported previously [28]. Details are presented in Supplementary materials and methods.

Measurement of the level of ubiquitinated p21

Details are presented in Supplementary materials and methods.

Reanalysis of public database records

RNA-seq datasets of 366 HCC tissues were downloaded from the National Cancer Institute website (https://www.cancer.gov/about-nci/organization/ccg/research/structural-genomics/tcga). Reads per million mapped reads (RPMs) for each dataset were processed and analyzed. Nineteen cases with a high expression level of *TERT* mRNA (RPM > 100.0) and 29 cases without *TERT* mRNA expression (RPM = 0.0) were selected as $TERT^{high}$ and $TERT^{null}$, respectively. Pathway analysis was conducted using DAVID Bioinformatics Resources software with default settings.

Statistics

Statistical analyses were performed using R version 4.1.2. Categorical values were analyzed using Fisher's exact test, whereas continuous values were analyzed using the Wilcoxon rank-sum test or Welch two-sample *t*-test. The Kruskal–Wallis test was used to compare three or more groups.

Results

A mouse model with liver-specific TERT overexpression

To investigate the *Tert* function in the liver *in vivo*, we generated a mouse model with liver-specific *Tert* overexpression using the *Cre-loxP* system by crossing *Tert*cTg mice with transgenic mice carrying the *Cre* gene under the control of an *Albumin* promoter (*Alb-Cre;Tert*Tg) (Figure 1A). Overexpression of *Tert* mRNA in the liver tissue was confirmed by RT-qPCR (Figure 1B). *Alb-Cre;Tert*Tg mice showed normal systemic development. The body and the liver weights of *Alb-Cre;Tert*Tg mice were comparable to those of the control mice (*Tert*cTg) (supplementary material, Figure S1A). There was no difference in the liver tissue macroscopically or histologically between control mice and *Alb-Cre;Tert*Tg mice, at both 4 and 48 weeks of age (Figure 1C and supplementary material, Figure S1B). Spontaneous tumor development was not detected in mice with either genotype at the age of 48 weeks.

Telomere shortening was paradoxically accelerated in the liver of *Alb-Cre;TertTg* mice under chronic inflammation

Although TERT is a component of telomerase, it remains unclear whether TERT overexpression causes telomere elongation. Thus, we examined the telomere length of cells collected from the livers of the control mice and *Alb-Cre;Tert*Tg mice. In the tissues of 4-week-old mice, telomere length was almost the same for both phenotypes. However, in the liver tissues of mice with chronic inflammation induced by 0.02% TAA for 50 weeks, unexpectedly, telomere length became shorter in *Alb-Cre;Tert*Tg than in control mice (Figure 1D). These results indicate that *Alb-Cre;Tert*Tg mice presented significant shortening of telomere length in the liver under chronic inflammation, suggesting that TERT has noncanonical roles independent of telomere maintenance.

Tert overexpression under chronic inflammation upregulated gene sets related to NFκB, cell cycle, and apoptosis pathway

We examined the phenotype of *Alb-Cre;Tert*Tg mice ($N = 25$) and control mice ($N = 28$) treated with 0.02% TAA for up to 30 weeks. Macroscopically, mild irregularities were observed on the liver surface of both groups. Pathologically, similar levels of inflammation and fibrosis were observed in both genotypes (Figure 2A, supplementary material, Table S4). Liver weight was also similar in both genotypes, in either

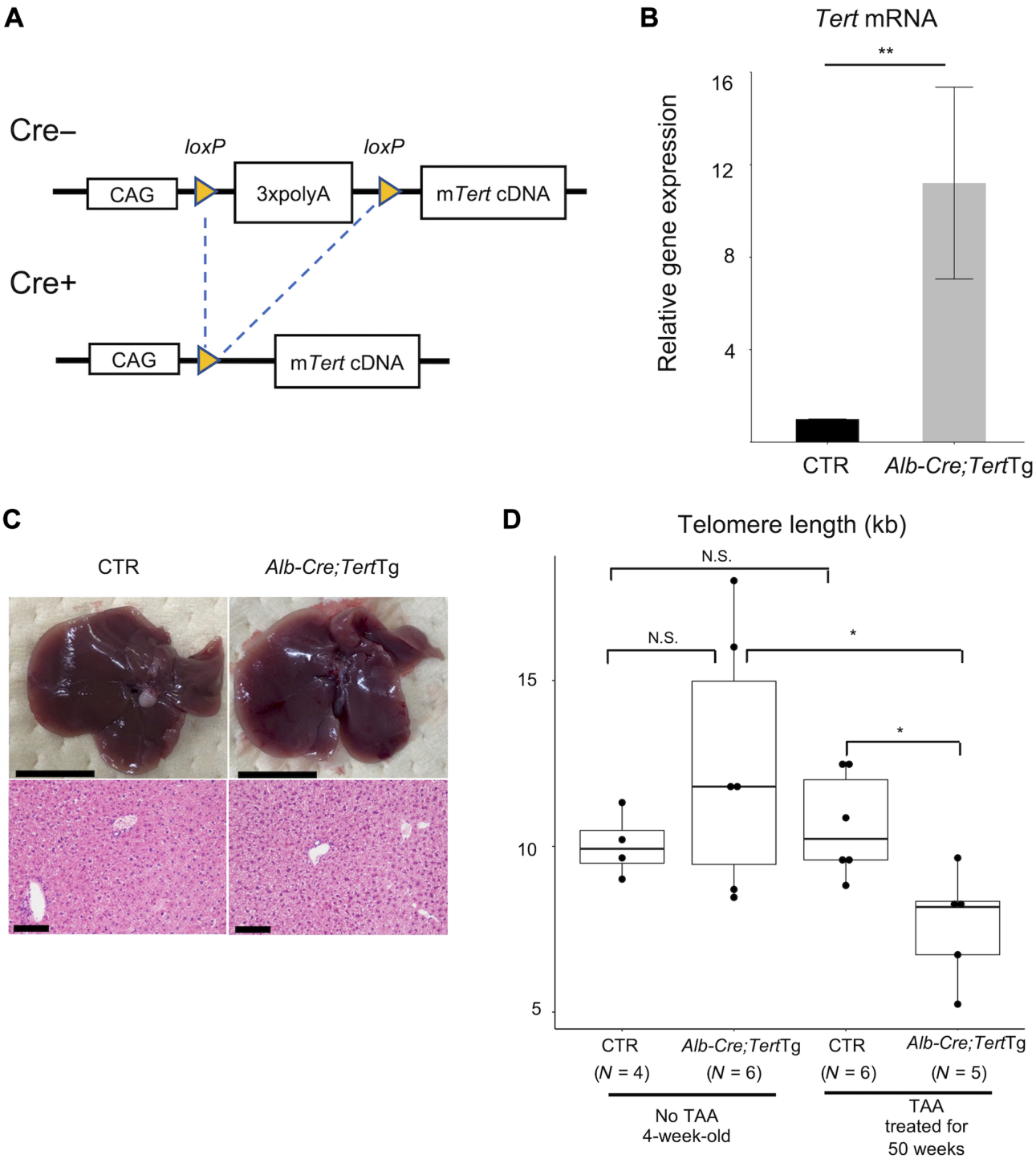

Figure 1. Mouse model with liver-specific *TERT* overexpression. (A) Structure of transgenes used to generate *Tert* conditional transgenic mice and structure after Cre-mediated recombination allowing the expression of *Tert* cDNA driven by the CAG promoter. Yellow triangles indicate *loxP* sites. (B) Relative expression level of *Tert* gene in primary hepatocytes of control mice and *Alb-Cre;Tert*Tg mice at 4 weeks of age. $N = 3$ for both genotypes. Data are presented as mean ± SD. $^{**}p < 0.01$. (C) Representative macroscopic appearance (upper panels, scale bar: 10 mm) and histological images stained with hematoxylin and eosin (lower panels, scale bar: 100 μm) of liver collected from a control mouse and an *Alb-Cre;Tert*Tg mouse at 4 weeks of age. (D) Comparison of telomere lengths between control mice and *Alb-Cre;Tert*Tg mice at 4 weeks of age or with TAA treatment for 50 weeks. $^{*}p < 0.05$. CTR, control; N.S., not significant. Created with R version 4.1.2.

absolute terms or relative to body weight (supplementary material, Figure S2A). Liver tumor development was observed in 28.0% (7/25) and 17.9% (5/28) of *Alb-Cre;Tert*Tg mice and control mice, respectively, but the difference between the two groups was not significant (Figure 2B). These phenotypes remained almost identical when the duration of TAA administration was extended to 50 weeks (supplementary material, Figure S2B–D and Table S5). To examine the changes in gene expression caused by *Tert* overexpression,

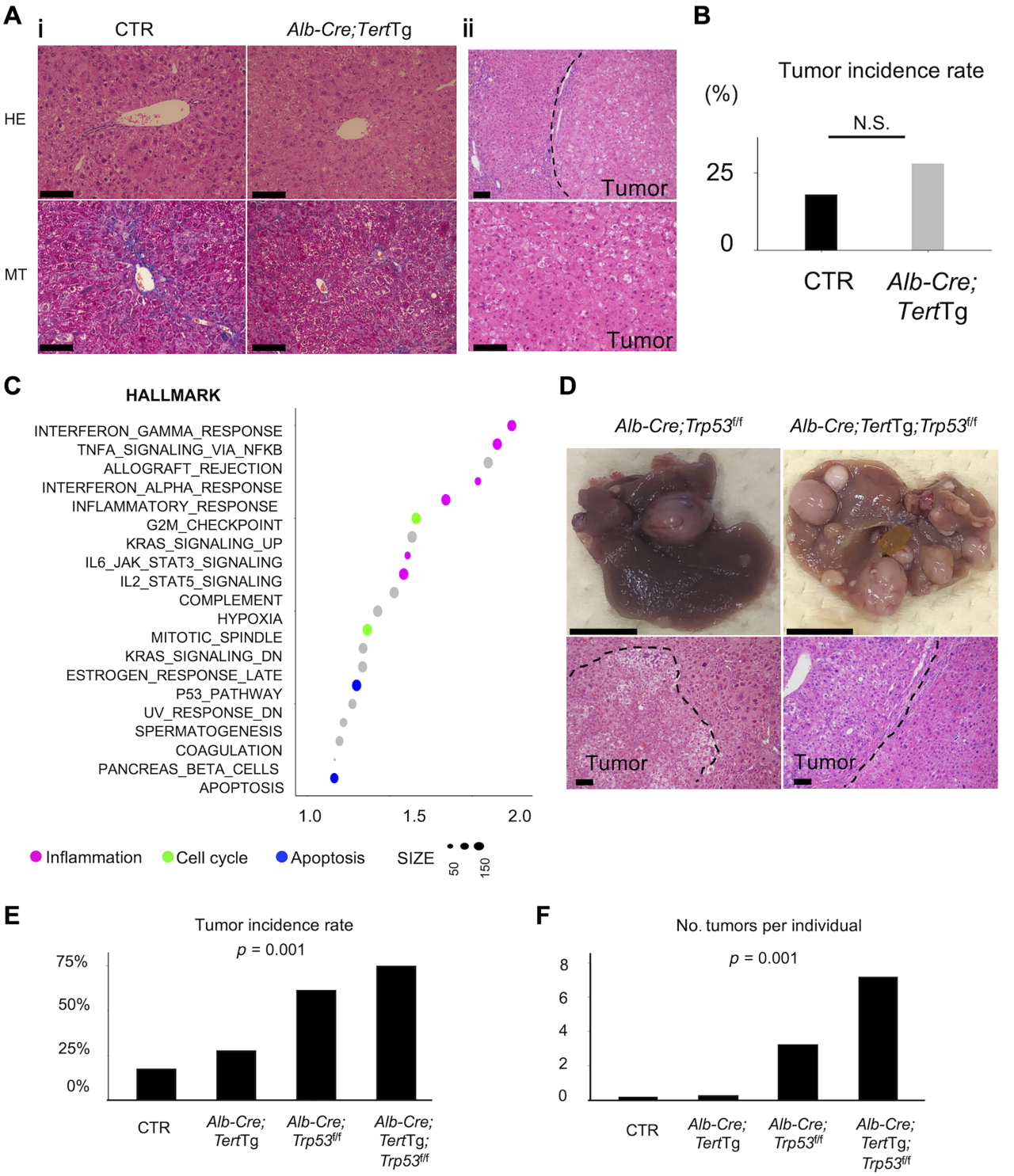

Figure 2. *Tert* overexpression under chronic inflammation increased tumorigenic potential. (A) (i) Representative images of noncancerous liver tissues stained with hematoxylin and eosin (HE) (upper panels, scale bar: 100 μm) and Masson's Trichrome (lower panels, scale bar: 100 μm). Both a control mouse and an *Alb-Cre;Tert*Tg mouse were treated with 0.02% TAA for 30 weeks. (ii) Representative HE staining images of liver tumors developed in an *Alb-Cre;Tert*Tg mouse after 30 weeks of 0.02% TAA treatment. A dotted line indicates a border between regions of tumor and nontumor (upper panel, scale bar: 100 μm; lower panel, scale bar: 100 μm). (B) The percentage of mice in which liver tumors were detected after 0.02% TAA treatment for up to 30 weeks. $N = 28$ for control and $N = 25$ for *Alb-Cre;Tert*Tg. p value was determined using Fisher's exact test. N.S., not significant. (C) Normalized enrichment score of HALLMARK gene sets significantly enriched in noncancerous liver tissues of *Alb-Cre;Tert*Tg mice ($N = 6$; male = 3, female = 3) compared with control mice ($N = 4$; male = 3, female = 1) after TAA treatment for up to 30 weeks. Gene sets related to inflammation, cell cycle, and apoptosis pathway are shown in pink, green, and blue, respectively. Cut-off of FWER p value is 0.02. (D) Representative macroscopic appearance (upper panels, scale bar: 10 mm) and histological images with HE staining of liver sections (lower panels, scale bar: 100 μm) collected from *Alb-Cre;Trp53*$^{f/f}$ mouse and *Alb-Cre;Tert*Tg;*Trp53*$^{f/f}$ mouse after 0.02% TAA treatment for 30 weeks. Dotted lines indicate border between regions of tumor and nontumor. Scale bar: 10 mm. (E) The tumor incidence rate and (F) the number of liver tumors per individual in control, *Alb-Cre;Tert*Tg, *Alb-Cre;Trp53*$^{f/f}$, and *Alb-Cre;Tert*Tg;*Trp53*$^{f/f}$ mice after 0.02% TAA treatment for up to 30 weeks. p values were determined by Kruskal–Wallis test in both (E) and (F). CTR, control; N.S., not significant, NES, normalized enrichment score. Created with R version 4.1.2.

we performed RNA-seq using noncancerous liver tissue samples from control ($N = 4$) and *Alb-Cre;Tert*Tg mice ($N = 6$) treated with TAA for up to 30 weeks. GSEA revealed that several gene sets associated with inflammatory carcinogenesis were significantly upregulated in *Tert*-overexpressed liver tissue followed by TAA treatment, including gene sets related to TNF-NFκB signaling, cell cycle progression, and apoptosis (Figure 2C). Together, under chronic inflammation, *Tert* overexpression did not increase the incidence of liver tumors but upregulated several gene sets involved in inflammatory carcinogenesis in liver tissues.

Tert overexpression worked oncogenically in the absence of Trp53

The enrichment of gene sets associated with apoptosis by *Tert* overexpression led us to speculate that *Tert* may promote tumorigenesis under conditions of *Trp53* loss because *TP53* is one of the most frequently altered genes in human HCC along with *TERT* [14]. To test this hypothesis, we generated a mouse model with liver-specific *Trp53* deletion and *Tert* overexpression: *Alb-Cre;Tert*Tg;*Trp53*$^{f/f}$ mice. The deletion of *Trp53* in the liver tissues was confirmed by RT-qPCR (supplementary material, Figure S3A). They developed multiple liver tumors more frequently than other mice after treatment with 0.02% TAA up to 30 weeks (Figure 2D,E and supplementary material, Table S4). The number of liver tumors per mouse also increased in them (Figure 2F). At the age of 90 weeks, *Alb-Cre;Tert*Tg;*Trp53*$^{f/f}$ mice spontaneously developed liver tumors, whereas no liver tumors were observed in *Alb-Cre;Trp53*$^{f/f}$ mice, indicating that TERT tended to promote tumorigenesis even without inflammatory stimulation (supplementary material, Figure S3B). These results suggested that TERT overexpression promoted tumorigenesis, particularly in the absence of adequate p53 function.

TERT had an enhancing effect on NFκB promoter activity

Next, we explored the role of TERT in hepatocarcinogenesis based on the results of the transcriptome analysis using human hepatoma cell lines. Because TERT is highly expressed in most hepatoma cell lines, we analyzed the function of TERT using gene silencing experiments. Among the gene sets upregulated by *Tert* overexpression under chronic inflammation, we first focused on TNF-NFκB signaling-related genes because they were also upregulated in the liver tissues of 48-week-old *Alb-Cre;Tert*Tg mice without TAA treatment (supplementary material, Figure S4A), suggesting that TERT could intrinsically affect the activity of the NFκB pathway. To assess the function of TERT on NFκB activity *in vitro*, we silenced TERT expression using siRNA specific to *TERT* (siTERT) in the human HCC cell lines HepG2 and Huh7 (Figure 3A,B and supplementary material, Figure S4B). By transfecting the cells with siTERT followed by a luciferase reporter plasmid containing a cis reporter of NFκB, NFκB promoter activity was measured with or without TERT knockdown (Figure 3C). As shown in Figure 3D, the NFκB promoter activity was substantially repressed in the cells treated with siTERT. As previously reported in ovarian carcinoma cell lines [18], the direct interaction between TERT protein and NFκB p65 subunit was confirmed by immunoprecipitation in HepG2 cells as well (Figure 3E). Immunohistochemistry for NFκB p65 using liver tissue from 48-week-old mice revealed that the expression of nuclear NFκB p65 was observed more frequently in hepatocytes of *Alb-Cre;Tert*Tg mice ($N = 3$) than in those of *Tert*Tg mice ($N = 3$) (Figure 3F,G). This aligns with the finding that TERT binds to the NFκB promoter and increases its activity. Collectively, TERT had an enhancing effect on NFκB promoter activity along with direct interaction with NFκB p65 and contributed to the augmentation of inflammation.

TERT drives cell cycle progression *in vitro* and *in vivo*

We examined the proliferation of human hepatoma cell lines after TERT silencing to investigate the function of TERT in regulating the cell cycle. The cell proliferation significantly decreased by TERT knockdown (Figure 4A). Flow cytometric analysis revealed that the proportion of cells in the S phase of the cell cycle was markedly decreased in the group treated with siTERT, but not in the G0/1 and G2/M phases (Figure 4B,C and supplementary material, Figure S5A,B). Consistent with this result, immunoblotting showed that all cyclins (A2/B1/D2/E) were downregulated by TERT knockdown (Figure 4D). Immunohistochemistry revealed that the number of hepatocytes stained with Ki67 and phosphorylated Rb was significantly increased in the livers of *Alb-Cre;Tert*Tg mice compared to that in control mice (Figure 4E,F). These findings indicated that elevated TERT expression could contribute to cell cycle progression.

TERT promoted the ubiquitin-mediated degradation of p21 dependent on CUL1 in G1/S phase

As *TERT* knockdown reduced the expression of multiple cyclins, we considered the possibility that TERT interacted with the cyclin-dependent kinase (CDK) inhibitor p21, which functions as a universal regulator of the cell cycle. The expression level of p21 protein in HepG2 cells was increased by TERT knockdown (Figure 5A). The expression level of the p21 protein was repressed in primary hepatocytes from *Alb-Cre;Tert*Tg mice treated with TAA for 30 weeks compared to those from control mice (Figure 5B). The *p21* (*Cdkn1a*) mRNA in the liver of *Alb-Cre;Tert*Tg mice did not decrease, contrary to p21 protein levels, with or without TAA treatment (supplementary material, Figure S6A,B), strongly suggesting that TERT interferes with p21 expression via post-transcriptional modifications. To examine whether TERT directly

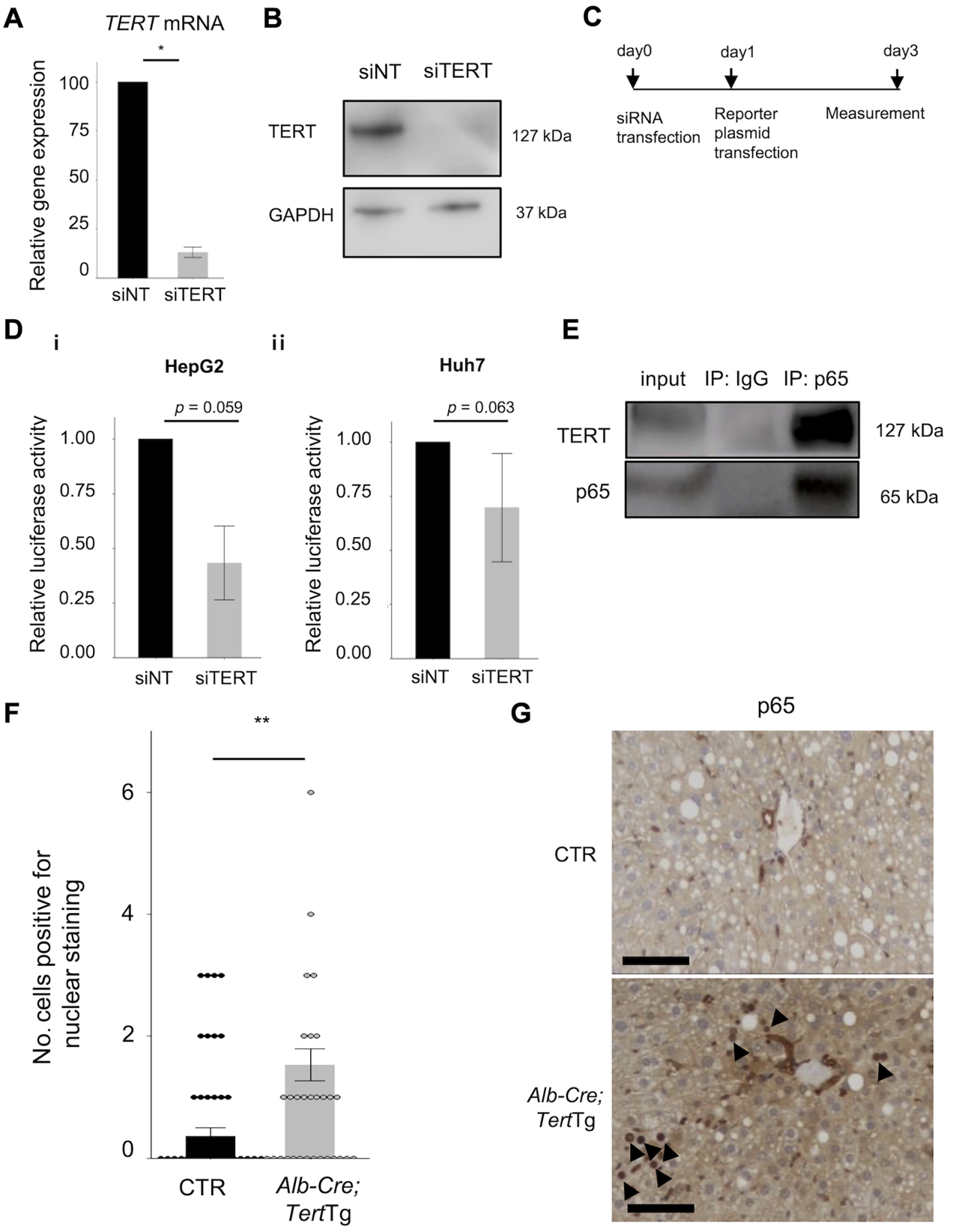

Figure 3. TERT had an enhancing effect on NFκB promoter activity. (A) Relative expression level of *TERT* gene with siNT and siTERT in HepG2. *p* values were determined by Welch's two-sample *t*-test. Data are presented as mean ± SD, $*p < 0.05$. (B) Immunoblotting analysis for TERT and GAPDH in HepG2 with siNT and siTERT. (C) Protocol of plasmid transfection and measurement of luciferase activity. (D) Relative luciferase activity in (i) HepG2 cells and (ii) Huh7 cells quantifying endogenous NFκB promoter activities. *p* values were determined by Welch's two-sample *t*-test. (E) Immunoblotting analysis for TERT and NFκB p65 in HepG2 cell lysates after immunoprecipitation using anti NFκB p65 antibody. (F) Bar chart shows number of NFκB p65-positive cells in liver tissue of *Tert*Tg mice ($N = 3$) and *Alb-Cre;Tert*Tg mice ($N = 3$). (G) Representative images of immunohistochemistry for NFκB p65 staining in liver tissue of *Tert*Tg mice and *Alb-Cre;Tert*Tg mice (scale bar: 100 μm). Data are presented as mean ± SEM. $**p < 0.01$. siNT, nontargeting control; siTERT, siRNA specific to TERT. Created with R version 4.1.2.

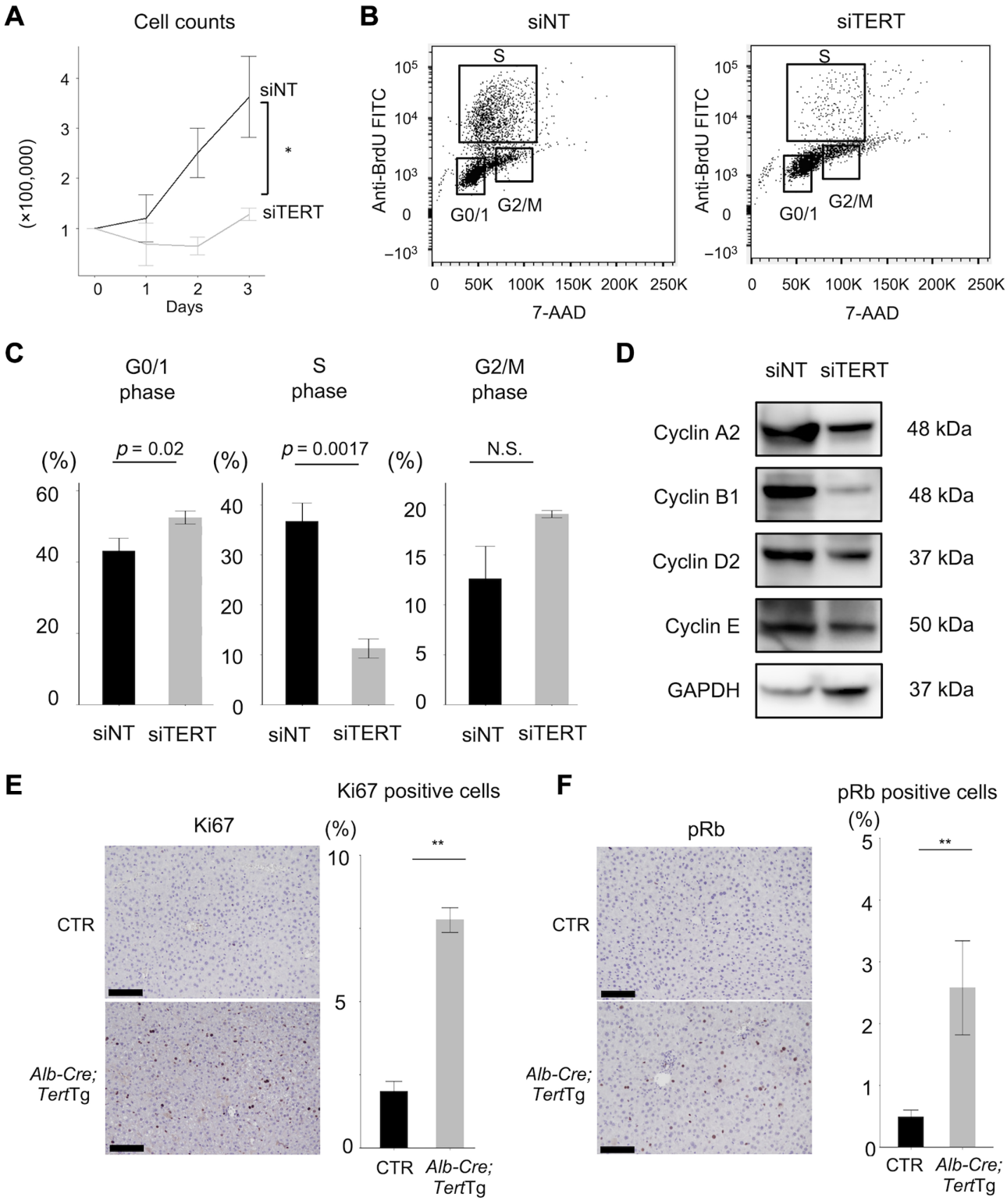

Figure 4. TERT drove cell cycle progression *in vitro* and *in vivo*. (A) Cell proliferation assay using HepG2 cells with siNT and siTERT. One hundred thousand cells per well were plated in six-well plates, and the number of cells from independent experimental wells was counted every 24 h. *p* values were determined by Welch's two-sample *t*-test. $*p < 0.05$. $N = 3$ for both groups. (B) Flow-cytometric analysis of HepG2 cells stained using Anti-BrdU-FITC and 7-AAD after transfection of siNT or siTERT. $N = 3$ for both groups. (C) The proportions of cells in G0/1, S-, and G2-phase as detected using flow cytometry analysis are shown in panels at left, middle, and right, respectively. *p* values were determined by Welch's two-sample *t*-test. Data are presented as mean ± SD. $*p < 0.05$, $**p < 0.01$. $N = 3$ for both groups. (D) Immunoblotting analysis for cyclin A2, cyclin B1, cyclin D2, cyclin E, and GAPDH using lysates of HepG2 cells transfected with siNT or siTERT. (E) Representative images of immunostaining for Ki67 in liver sections of a control mouse and an *Alb-Cre;Tert*Tg are shown (scale bar: 100 μm). Bar chart shows percentage of Ki67-positive cells in liver tissue of control mouse and *Alb-Cre;Tert*Tg mouse. (F) Representative images of immunostaining for phosphorylated-Rb (pRb) in liver sections of control mouse and *Alb-Cre;Tert*Tg are shown (scale bar: 100 μm). Bar chart shows percentage of pRb-positive cells in liver tissue of control mouse and *Alb-Cre;Tert*Tg mouse. *p* values were determined by Welch's two-sample *t*-test. Data presented as mean ± SD. $**p < 0.01$ in both (E) and (F). siNT, nontargeting control; siTERT, siRNA specific to TERT; CTR, control; N.S., not significant. Created with R version 4.1.2.

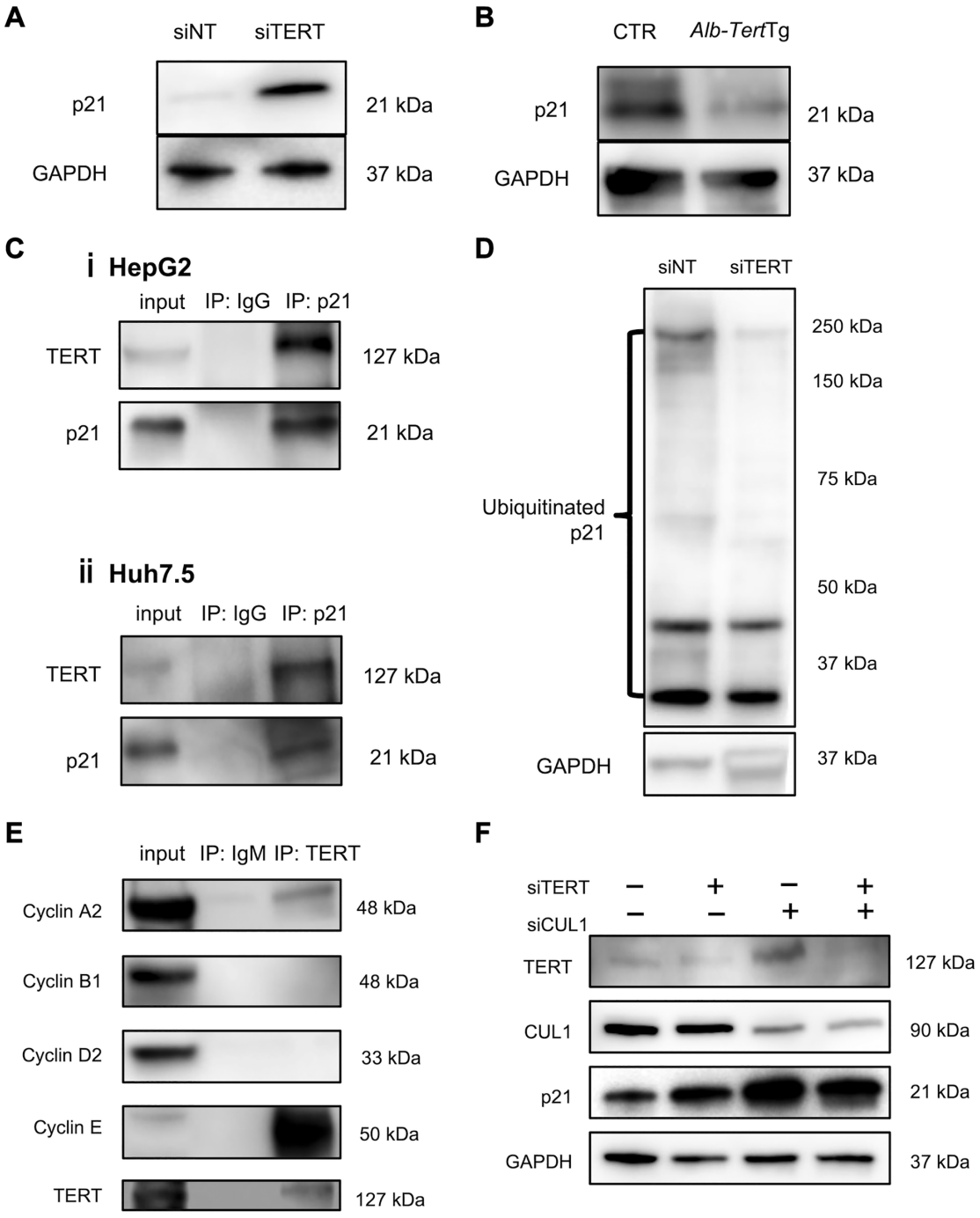

Figure 5. TERT promoted ubiquitin-mediated degradation of p21 dependent on CUL1 in G1/S phase. (A) Immunoblotting analysis for p21 and GAPDH in lysates of HepG2 cells transfected with siNT or siTERT. (B) Immunoblotting analysis for p21 and GAPDH in lysates of primary hepatocytes from control mouse and *Alb-Cre;Tert*Tg mouse after 0.02% TAA treatment for 30 weeks. (C) Immunoblotting analysis for TERT and p21 in (i) HepG2 cell lysates and (ii) Huh7.5 cell lysates after immunoprecipitation using anti-p21 antibody. (D) Detection of ubiquitinated p21 by immunoblotting analysis in lysates of HepG2 treated with MG132. (E) Immunoblotting analysis for cyclin A2, cyclin B1, cyclin D2, cyclin E, and TERT in HepG2 cell lysates after immunoprecipitation using anti-TERT antibody. (F) Immunoblotting analysis for TERT, CUL1, p21, and GAPDH in HepG2 cell lysates after transfection of siTERT and/or siCUL1. CTR, control. siNT, nontargeting control; siTERT, siRNA specific to TERT; siCUL1, siRNA specific to CUL1.

interacted with p21, immunoprecipitation analysis was performed. We found that TERT and p21 directly bound to each other (Figure 5C). We considered that this inhibitory effect of TERT on p21 might occur through the ubiquitin–proteasome system because the expression of the p21 protein is regulated by ubiquitin-mediated degradation, which occurs during the cell cycle [29,30]. To test this hypothesis, we examined the amount of ubiquitinated p21 in cell lysates of cells treated with MG132 by immunoblotting. The ubiquitinated p21 level was decreased by TERT silencing (Figure 5D), indicating that

TERT expression promoted p21 ubiquitination and contributed to p21 protein degradation. To verify the molecules included in the TERT–p21 complex, we performed co-immunoprecipitation and found that TERT bound to cyclin A2 and cyclin E but not to cyclin B1 or cyclin D2 (Figure 5E). As p21 forms a

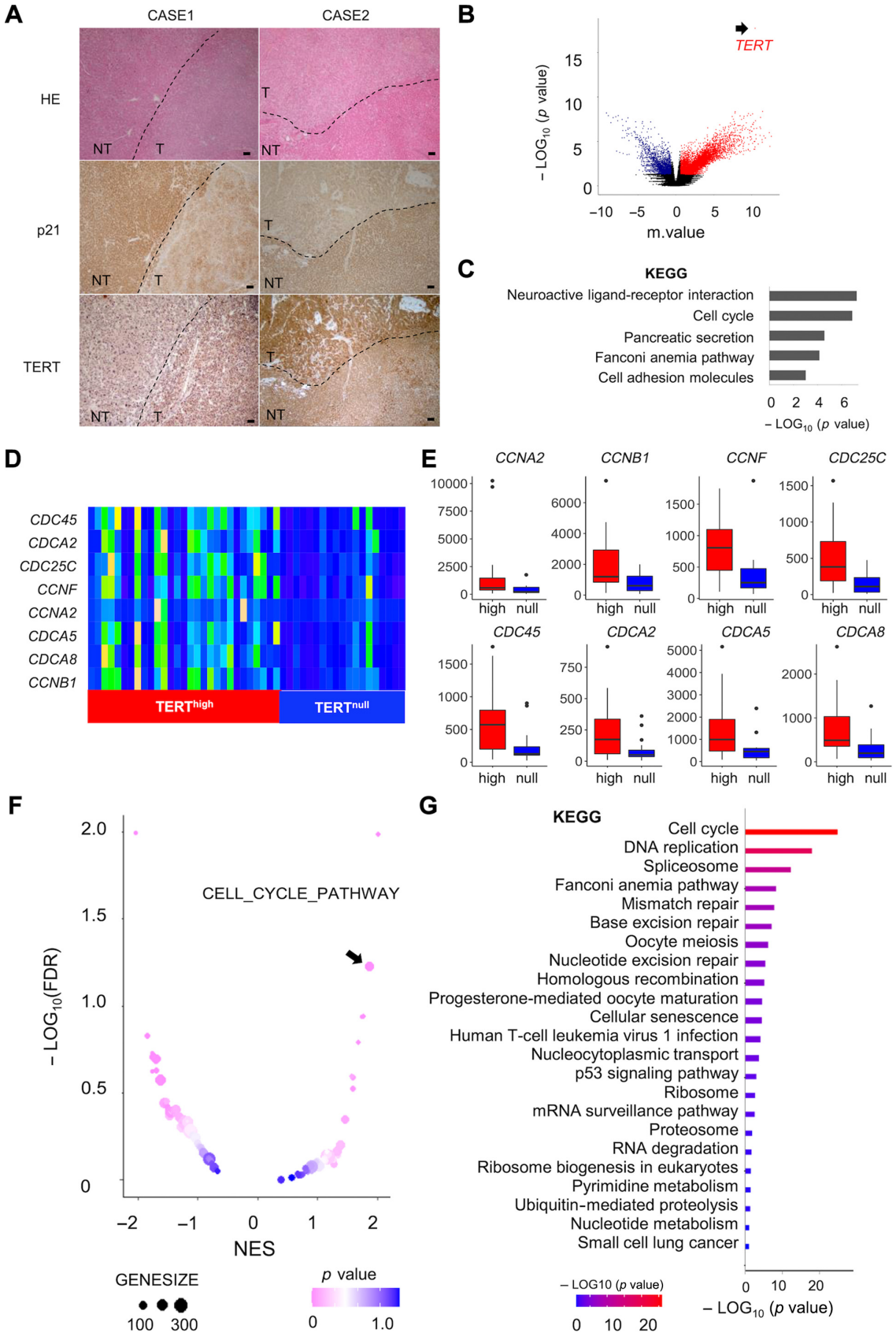

Figure 6 Legend on next page.

protein complex with cyclin A and cyclin E in the G1 phase [30], we hypothesized that TERT might guide the p21–cyclin A/E complex to ubiquitin-mediated proteolysis induced by CUL1, which consists of an E3 ubiquitin ligase complex that specifically acts in the G1 phase for p21 degradation [31]. Indeed, p21 expression increased when the cells were treated with siTERT, CUL1 siRNA (siCUL1), or both (Figure 5F). Taken together, these data support that TERT directly interacts with the p21 protein and promotes the ubiquitin-mediated degradation of p21 dependent on CUL1, leading to cell cycle progression, especially in the G1/S phase.

Human HCCs with TERT upregulation are associated with downregulation of p21 and upregulation of cell-cycle-related genes

To verify the relationship between TERT and p21 in a clinical setting, we examined the protein expression levels of p21 and TERT using immunohistochemistry in liver tissues of patients with HCC surgically resected at Kyoto University Hospital. Consistent with the results of our experiments, higher TERT expression and lower p21 expression were observed in HCC tissues than in noncancerous tissues (Figure 6A). We also examined gene expression profiles associated with TERT expression in human HCC samples using The Cancer Genome Atlas (TCGA) database. We identified 3,275 DEGs between $TERT^{high}$ HCCs and $TERT^{null}$ HCCs using edgeR (false discovery rate < 0.05) (Figure 6B and supplementary material, Table S6). Pathway analysis performed for the DEGs using DAVID revealed that the pathway related to the cell cycle appeared in the top five gene sets (Figure 6C). Indeed, several well-known genes important for cell cycle progression were included in the DEGs (Figure 6D,E). GSEA also demonstrated that the gene set related to the cell cycle was upregulated in the $TERT^{high}$ group (Figure 6F and supplementary material, Figure S7A,B). Furthermore, a total of 1,077 genes were extracted from the RNA-seq data of 366 HCC cases in TCGA database that correlated with TERT expression ($r > 0.2$) (supplementary material, Table S7). Pathway analysis using these genes revealed that the cell-cycle-related pathway was the most upregulated (Figure 6G). Taken together, TERT expression showed an inverse correlation with p21 expression, which could be related to accelerated cell cycle progression in human HCCs.

Discussion

TERT is the most frequently mutated gene in human HCC tissues. It is transcriptionally silenced in normal differentiated cells, whereas an aberration of *TERT* leads to gene upregulation [7,32,33]. Telomerase consists of the TERT protein and telomere RNA component (TERC) and maintains telomere length by adding six bases, TTAGGG, to the 3'-end of shortened telomeres after cell division. Therefore, it has been considered that TERT reactivation would contribute to cell immortalization in cancer tissues [10,33].

In the current study, we generated a mouse model of liver-specific *Tert* overexpression, *Alb-Cre;Tert*Tg, and examined its phenotype to elucidate the role of TERT upregulation in hepatocarcinogenesis. Although telomere length was almost comparable in the liver between *Alb-Cre;Tert*Tg and control mice without inflammatory stimulation, telomeres became paradoxically short in *Alb-Cre;Tert*Tg livers under the conditions of chronic inflammation, suggesting that high expression levels of TERT in hepatocytes with chronic inflammation lead to telomere shortening by an unknown mechanism. This unanticipated result prompted us to explore the noncanonical role of TERT in hepatocytes independent of telomere maintenance.

Various functions, other than telomere maintenance, have been reported for TERT. TERT interacts with several key molecules, such as β-catenin and BRG1. TERT–β-catenin interaction activates resting hair [34] and epithelial stem cells [35]. TERT interacts with BRG1 in a Wnt/β-catenin-dependent manner; however, the role of this interaction is largely unknown and may be strongly context dependent [36]. Sharma *et al* reported that TERT was localized in the mitochondria and acted as a reverse transcriptase for mitochondrial RNA without carrying TERC [37]. TERT also displays a RNA-dependent RNA polymerase (RdRP) activity and produces double-stranded RNAs that are processed into small interfering RNA [38]. Phosphorylation of threonine 249 of TERT by CDK1 regulates RdRP activity and contributes to cancer progression independent of the telomeric effect [39]. In the current study, as genes associated with TNF–NFκB signaling were highly upregulated in *Alb-Cre;Tert*Tg liver, even without inflammatory stimulation, we examined the activity of NFκB in HCC cells with TERT upregulation and confirmed that TERT directly interacted with p65 subunit, leading to the increase of the NFκB promoter activity,

Figure 6. In human HCCs, TERT upregulation was associated with downregulation of p21 and upregulation of cell-cycle-related genes. (A) Representative images of HCC samples stained with HE (left panels), immunostained for p21 (middle panels) and TERT (right panels) (scale bar: 100 μm). (B) DEGs of $TERT^{high}$ HCC and $TERT^{null}$ HCC are shown in a volcano plot. Genes with m.value < and m.value >0.6 and p value < 0.05 or m.value < −0.6 and p value < 0.05 are shown in red and blue, respectively. (C) KEGG gene sets enhanced in $TERT^{high}$ HCC using DAVID. (D) Heatmap showing RNA expression of representative eight cell-cycle-related genes in $TERT^{high}$ and $TERT^{null}$ groups. (E) Expression levels of cell-cycle-related genes in $TERT^{high}$ and $TERT^{null}$ groups. (F) Normalized enrichment score of KEGG gene sets enriched in $TERT^{high}$ group detected through GSEA. (G) KEGG gene sets that fluctuate in correlation with TERT expression changes using DAVID. high, $TERT^{high}$; null, $TERT^{null}$. Created with R version 4.1.2.

which is one of the most important signaling pathways in HCC development. Our data are consistent with previous findings that telomerase directly controls NFκB-dependent gene expression by binding to the NFκB p65 subunit and contributes to inflammation and cancer progression [18].

In contrast, we found that TERT overexpression also resulted in the upregulation of genes related to cell cycle progression in transcriptome analysis using the *Alb-Cre;Tert*Tg model. The increase in the S-phase population and enhancement of proliferative activity in *TERT*-upregulated hepatoma cells *in vitro* led us to assume that TERT had a noncanonical function related to cell cycle progression, which could explain why telomere shortening was promoted in *Alb-Cre;Tert*Tg mice under chronic inflammation. TERT is involved in the downregulation of CDK inhibitors; however, the underlying mechanism remains unelucidated [40]. As the expression levels of multiple cyclins were decreased by TERT silencing, we focused on the CDK inhibitor p21. p21 is encoded by *CDKN1A* and is involved in cell proliferation signaling in response to various stimuli by binding to and inactivating CDKs [30,41–43]. CDK inhibition by p21 triggers cell-cycle arrest in the G1 and G2 phases of the cell cycle [30]. p21 is negatively regulated by the ubiquitin–proteasome system; in particular, the E3 ubiquitin ligase complex SKP1-CUL1-SKP2 promotes the degradation of p21 combined with CDK2 and cyclin A/E in the G1 phase [31,44–47]. We revealed that TERT directly bound to the p21 protein and inhibited its function in cell cycle arrest by promoting its degradation via the ubiquitin–proteasome system, leading to cell proliferation. The inverse correlation between TERT and p21 expression observed in human HCC samples corroborated the results *in vitro* and *in vivo*. TERT is considered to interact with p21 specifically in the G1 phase because it binds to cyclin A2/E and not to cyclin B1/D2. The mechanism by which TERT suppresses p21 expression in the G1 phase needs to be elucidated in future studies.

We found that *Alb-Cre;Tert*Tg;*Trp53*$^{f/f}$ mice developed liver tumors more frequently than *Alb-Cre;Tert*Tg mice or *Alb-Cre;Trp53*$^{f/f}$ mice. These results indicated that the combination of *Tert* upregulation with *Trp53* loss promoted HCC development and recapitulated the human multistep hepatocarcinogenesis in which gene aberrations of *TERT* and *TP53* were crucial events in the early stage [11]. Indeed, the gene sets enriched in the liver of *Alb-Cre;Tert*Tg mice included those related to apoptosis, which might be a physiological response to the increased carcinogenic potential triggered by TERT upregulation. The present data suggested that, in the clinical course of HCC, the promotion of cell proliferation induced by TERT upregulation accompanied by a decrease of p21 expression might increase the carcinogenic potential and enhance apoptosis pathway, which is prone to HCC development by a second hit such as p53 loss.

Finally, we analyzed the molecular biological properties of HCCs with high expression of TERT using RNA-seq data of TCGA. Multiple genes related to cell cycle progression were enriched in HCC with TERT upregulation, suggesting that TERT expression is involved in cell cycle acceleration. These clinical data are consistent with our experimental results showing TERT promoted cell cycle entry via p21 degradation.

This study had limitations. First, the contribution of the TERT–p21 interaction to cell proliferation and prognosis was not validated in a large number of clinical cases owing to the absence of proteome data in the liver cancer cohort. Because p21 is also regulated by other molecules such as p53, it might be difficult to examine the pure correlation between TERT and p21 expression in HCC specimens, especially tumors harboring *TP53* mutations, which was observed in approximately 40% of cases with HCC [48]. However, as TERT expression may be one of the factors useful for classifying HCCs independent of other oncogenic pathways, further analysis in a large cohort is needed. Second, the possibility that the physiological difference in telomere length between mice and humans might have emphasized the noncanonical role of *TERT* independent of telomere maintenance in the phenotype of *Alb-Cre;Tert*Tg mice because mouse telomeres are much longer than human telomeres and will not be critically short even under inflammation.

In conclusion, the aberrant upregulation of TERT observed in the course of chronic liver inflammation could contribute to carcinogenesis by increasing NFκB promoter activity and by promoting cell cycle progression via ubiquitination of p21 protein, followed by a second hit, such as p53 loss, might promote hepatocarcinogenesis. This could be a reasonable explanation of why *TERT* aberrations leading to upregulation are observed so frequently in the early phase of hepatocarcinogenesis. This study provides a rationale for developing a novel therapeutic strategy of HCC targeting *TERT*.

Acknowledgements

The authors thank Drs. Yoshihide Ueda, Ken Takahashi, Tadashi Inuzuka, Haruka Amino, and Natsumi Oe for helpful suggestions. This work was supported by grants from Japan Society for the Promotion of Science (JSPS) Grants-in-Aid for Scientific Research, KAKENHI (17H04158, 19K08443, 21K07912, 22K07983, 22K15964).

Author contribution statement

MM, AT and HM conceived the study design. MM carried out all the experiments. TM conducted immunohistochemical staining and flow cytometry. HT, SN and EH collected the clinical samples. MM, AT, HT and TM performed sequencing analysis and interpreted the data. SH and KN provided administrative, technical or material support. MM and AT wrote the manuscript, and HT, EI, YF, MU, TI, MT, YE, TS, TM and SH provided critical revision of the manuscript for intellectual

content. AT and HS supervised the study. All authors approved the final version of the manuscript.

Data availability statement

The data that support the findings of this study are openly available in the DDBJ Sequence Read Archive (DRA) at https://www.ddbj.nig.ac.jp/dra/index-e.html, the BioProject number: PRJDB16181.

References

1. Llovet JM, Kelley RK, Villanueva A, *et al*. Hepatocellular carcinoma. *Nat Rev Dis Primers* 2021; **7:** 6.
2. Villanueva A. Hepatocellular carcinoma. *N Engl J Med* 2019; **380:** 1450–1462.
3. Zucman-Rossi J, Villanueva A, Nault J-C, *et al*. Genetic landscape and biomarkers of hepatocellular carcinoma. *Gastroenterology* 2015; **149:** 1226–1239.e4.
4. Schulze K, Imbeaud S, Letouzé E, *et al*. Exome sequencing of hepatocellular carcinomas identifies new mutational signatures and potential therapeutic targets. *Nat Genet* 2015; **47:** 505–511.
5. Nault JC, Mallet M, Pilati C, *et al*. High frequency of telomerase reverse-transcriptase promoter somatic mutations in hepatocellular carcinoma and preneoplastic lesions. *Nat Commun* 2013; **4:** 2218.
6. Totoki Y, Tatsuno K, Covington KR, *et al*. Trans-ancestry mutational landscape of hepatocellular carcinoma genomes. *Nat Genet* 2014; **46:** 1267–1273.
7. Roake CM, Artandi SE. Regulation of human telomerase in homeostasis and disease. *Nat Rev Mol Cell Biol* 2020; **21:** 384–397.
8. Blackburn EH. Structure and function of telomeres. *Nature* 1991; **350:** 569–573.
9. Blackburn EH. Telomeres: no end in sight. *Cell* 1994; **77:** 621–623.
10. Strahl C, Blackburn EH. Effects of reverse transcriptase inhibitors on telomere length and telomerase activity in two immortalized human cell lines. *Mol Cell Biol* 1996; **16:** 53–65.
11. Takeda H, Takai A, Kumagai K, *et al*. Multiregional whole-genome sequencing of hepatocellular carcinoma with nodule-in-nodule appearance reveals stepwise cancer evolution. *J Pathol* 2020; **252:** 398–410.
12. Castelo-Branco P, Choufani S, Mack S, *et al*. Methylation of the TERT promoter and risk stratification of childhood brain tumours: an integrative genomic and molecular study. *Lancet Oncol* 2013; **14:** 534–542.
13. Kyo S, Takakura M, Fujiwara T, *et al*. Understanding and exploiting hTERT promoter regulation for diagnosis and treatment of human cancers. *Cancer Sci* 2008; **99:** 1528–1538.
14. Fujimoto A, Furuta M, Shiraishi Y, *et al*. Whole-genome mutational landscape of liver cancers displaying biliary phenotype reveals hepatitis impact and molecular diversity. *Nat Commun* 2015; **6:** 6120.
15. Nault JC, Calderaro J, Di Tommaso L, *et al*. Telomerase reverse transcriptase promoter mutation is an early somatic genetic alteration in the transformation of premalignant nodules in hepatocellular carcinoma on cirrhosis. *Hepatology* 2014; **60:** 1983–1992.
16. Kim SK, Takeda H, Takai A, *et al*. Comprehensive analysis of genetic aberrations linked to tumorigenesis in regenerative nodules of liver cirrhosis. *J Gastroenterol* 2019; **54:** 628–640.
17. Li Y, Tergaonkar V. Noncanonical functions of telomerase: implications in telomerase-targeted cancer therapies. *Cancer Res* 2014; **74:** 1639–1644.
18. Ghosh A, Saginc G, Leow SC, *et al*. Telomerase directly regulates NF-κB-dependent transcription. *Nat Cell Biol* 2012; **14:** 1270–1281.
19. Ghareghomi S, Ahmadian S, Zarghami N, *et al*. Fundamental insights into the interaction between telomerase/TERT and intracellular signaling pathways. *Biochimie* 2021; **181:** 12–24.
20. Hidema S, Fukuda T, Date S, *et al*. Transgenic expression of telomerase reverse transcriptase (Tert) improves cell proliferation of primary cells and enhances reprogramming efficiency into the induced pluripotent stem cell. *Biosci Biotechnol Biochem* 2016; **80:** 1925–1933.
21. Aoi T, Yae K, Nakagawa M, *et al*. Generation of pluripotent stem cells from adult mouse liver and stomach cells. *Science* 2008; **321:** 699–702.
22. Yoshida K, Sanada M, Shiraishi Y, *et al*. Frequent pathway mutations of splicing machinery in myelodysplasia. *Nature* 2011; **478:** 64–69.
23. Kakiuchi N, Yoshida K, Uchino M, *et al*. Frequent mutations that converge on the NFKBIZ pathway in ulcerative colitis. *Nature* 2020; **577:** 260–265.
24. Sun J, Nishiyama T, Shimizu K, *et al*. TCC: an R package for comparing tag count data with robust normalization strategies. *BMC Bioinformatics* 2013; **14:** 219.
25. Subramanian A, Tamayo P, Mootha VK, *et al*. Gene set enrichment analysis: a knowledge-based approach for interpreting genome-wide expression profiles. *Proc Natl Acad Sci U S A* 2005; **102:** 15545–15550.
26. Huang DW, Sherman BT, Lempicki RA. Systematic and integrative analysis of large gene lists using DAVID bioinformatics resources. *Nat Protoc* 2009; **4:** 44–57.
27. Iguchi E, Takai A, Takeda H, *et al*. DNA methyltransferase 3B plays a protective role against hepatocarcinogenesis caused by chronic inflammation via maintaining mitochondrial homeostasis. *Sci Rep* 2020; **10:** 21268.
28. Marusawa H, Hijikata M, Chiba T, *et al*. Hepatitis C virus core protein inhibits Fas- and tumor necrosis factor alpha-mediated apoptosis via NF-kappaB activation. *J Virol* 1999; **73:** 4713–4720.
29. Cai K, Dynlacht BD. Activity and nature of p21(WAF1) complexes during the cell cycle. *Proc Natl Acad Sci U S A* 1998; **95:** 12254–12259.
30. Abbas T, Dutta A. p21 in cancer: intricate networks and multiple activities. *Nat Rev Cancer* 2009; **9:** 400–414.
31. Yu ZK, Gervais JL, Zhang H. Human CUL-1 associates with the SKP1/SKP2 complex and regulates p21(CIP1/WAF1) and cyclin D proteins. *Proc Natl Acad Sci U S A* 1998; **95:** 11324–11329.
32. Yuan X, Larsson C, Xu D. Mechanisms underlying the activation of TERT transcription and telomerase activity in human cancer: old actors and new players. *Oncogene* 2019; **38:** 6172–6183.
33. Pestana A, Vinagre J, Sobrinho-Simões M, *et al*. TERT biology and function in cancer: beyond immortalisation. *J Mol Endocrinol* 2017; **58:** R129–R146.
34. Choi J, Southworth LK, Sarin KY, *et al*. TERT promotes epithelial proliferation through transcriptional control of a Myc- and Wnt-related developmental program. *PLoS Genet* 2008; **4:** e10.
35. Sarin KY, Cheung P, Gilison D, *et al*. Conditional telomerase induction causes proliferation of hair follicle stem cells. *Nature* 2005; **436:** 1048–1052.
36. Park BS, Song DH, Kim HM, *et al*. The structural basis of lipopolysaccharide recognition by the TLR4-MD-2 complex. *Nature* 2009; **458:** 1191–1195.
37. Sharma NK, Reyes A, Green P, *et al*. Human telomerase acts as a hTR-independent reverse transcriptase in mitochondria. *Nucleic Acids Res* 2012; **40:** 712–725.
38. Maida Y, Yasukawa M, Furuuchi M, *et al*. An RNA-dependent RNA polymerase formed by TERT and the RMRP RNA. *Nature* 2009; **461:** 230–235.
39. Yasukawa M, Ando Y, Yamashita T, *et al*. CDK1 dependent phosphorylation of hTERT contributes to cancer progression. *Nat Commun* 2020; **11:** 1557.

40. Xiang H, Wang J, Mao Y, *et al*. Human telomerase accelerates growth of lens epithelial cells through regulation of the genes mediating RB/E2F pathway. *Oncogene* 2002; **21:** 3784–3791.
41. Ball KL. p21: structure and functions associated with cyclin-CDK binding. *Prog Cell Cycle Res* 1997; **3:** 125–134.
42. Malumbres M, Barbacid M. Mammalian cyclin-dependent kinases. *Trends Biochem Sci* 2005; **30:** 630–641.
43. Malumbres M, Barbacid M. Cell cycle, CDKs and cancer: a changing paradigm. *Nat Rev Cancer* 2009; **9:** 153–166.
44. Bornstein G, Bloom J, Sitry-Shevah D, *et al*. Role of the SCFSkp2 ubiquitin ligase in the degradation of p21Cip1 in S phase. *J Biol Chem* 2003; **278:** 25752–25757.
45. Wang W, Nacusi L, Sheaff RJ, *et al*. Ubiquitination of p21Cip1/WAF1 by SCFSkp2: substrate requirement and ubiquitination site selection. *Biochemistry* 2005; **44:** 14553–14564.
46. Dang F, Nie L, Wei W. Ubiquitin signaling in cell cycle control and tumorigenesis. *Cell Death Differ* 2021; **28:** 427–438.
47. Bloom J, Amador V, Bartolini F, *et al*. Proteasome-mediated degradation of p21 via N-terminal ubiquitinylation. *Cell* 2003; **115:** 71–82.
48. Fujimoto A, Furuta M, Totoki Y, *et al*. Whole-genome mutational landscape and characterization of noncoding and structural mutations in liver cancer. *Nat Genet* 2016; **48:** 500–509.

SUPPLEMENTARY MATERIAL ONLINE

Supplementary materials and methods

Figure S1. Mouse model with liver-specific TERT overexpression

Figure S2. Tert overexpression under chronic inflammation upregulated gene sets related to NFκB, cell cycle, and apoptosis pathway

Figure S3. *Tert* overexpression worked oncogenically in the absence of *Trp53*

Figure S4. TERT had an enhancing effect on NFκB promoter activity

Figure S5. TERT drove cell cycle progression *in vitro* and *in vivo*

Figure S6. TERT promoted the ubiquitin-mediated degradation of p21 dependent on CUL1 in G1/S phase

Figure S7. Human HCCs with TERT upregulation were associated with the downregulation of p21 and upregulation of cell-cycle-related genes

Table S1. Primers for genotyping PCR

Table S2. List of antibodies

Table S3. Primers for qPCR

Table S4. Incidence of liver tumors observed in CTR, *Alb-Cre;Tert*Tg, *Alb-Cre;Trp53*$^{f/f}$, and *Alb-Cre;Tert*Tg;*Trp53*$^{f/f}$ mice with TAA treatment for up to 30 weeks

Table S5. Incidence of liver tumors observed in CTR and *Alb-Cre;Tert*Tg mice with TAA treatment for 50 weeks

Table S6. List of 3,275 DEGs

Table S7. Annotation clusters of 1,077 genes that fluctuated in correlation with TERT expression in the HCC cohort of the TCGA database